LETTERS
PUBLISHED ONLINE: 15 JUNE 2015 | DOI: 10.1038/NNANO.2015.118
nature nanotechnology

Bright visible light emission from graphene

Young Duck Kim[1,2*‡], Hakseong Kim[3‡], Yujin Cho[4‡†], Ji Hoon Ryoo[1‡], Cheol-Hwan Park[1], Pilkwang Kim[1], Yong Seung Kim[5], Sunwoo Lee[6], Yilei Li[6,7], Seung-Nam Park[8], Yong Shim Yoo[8], Duhee Yoon[4†], Vincent E. Dorgan[9†], Eric Pop[10], Tony F. Heinz[6,7†], James Hone[2], Seung-Hyun Chun[5], Hyeonsik Cheong[4], Sang Wook Lee[3], Myung-Ho Bae[8,11*] and Yun Daniel Park[1,12*]

Graphene and related two-dimensional materials are promising candidates for atomically thin, flexible and transparent optoelectronics[1,2]. In particular, the strong light–matter interaction in graphene[3] has allowed for the development of state-of-the-art photodetectors[4,5], optical modulators[6] and plasmonic devices[7]. In addition, electrically biased graphene on SiO_2 substrates can be used as a low-efficiency emitter in the mid-infrared range[8,9]. However, emission in the visible range has remained elusive. Here, we report the observation of bright visible light emission from electrically biased suspended graphene devices. In these devices, heat transport is greatly reduced[10]. Hot electrons (~2,800 K) therefore become spatially localized at the centre of the graphene layer, resulting in a 1,000-fold enhancement in thermal radiation efficiency[8,9]. Moreover, strong optical interference between the suspended graphene and substrate can be used to tune the emission spectrum. We also demonstrate the scalability of this technique by realizing arrays of chemical-vapour-deposited graphene light emitters. These results pave the way towards the realization of commercially viable large-scale, atomically thin, flexible and transparent light emitters and displays with low operation voltage and graphene-based on-chip ultrafast optical communications.

For the realization of graphene-based bright and broadband light emitters, the non-equilibrium electron–hole recombination in gapless graphene is not efficient because of the rapid energy relaxation that occurs through electron–electron and electron–phonon interactions[11–13]. On the other hand, graphene's superior strength[14] and high-temperature stability may enable efficient thermal light emission. However, the thermal radiation from electrically biased graphene supported on a substrate[8,9,15–17] has been found to be limited to the infrared range and to be inefficient, as an extremely small fraction of the applied energy ($\sim 10^{-6}$)[8,9] is converted into light radiation. Such limitations are the direct result of heat dissipation through the underlying substrate[18] and significant hot electron relaxation from dominant extrinsic scattering effects such as charged impurities[19] and the surface polar optical phonon interaction[20], thus limiting maximum operating temperatures.

Freely suspended graphene is largely immune to such undesirable vertical heat dissipation[10] and extrinsic scattering effects[21,22], and therefore promises much more efficient and brighter radiation in the infrared-to-visible range. Due to the strong Umklapp phonon–phonon scattering[23], we find that the thermal conductivity of graphene at high lattice temperatures (1,800 ± 300 K) is greatly reduced (~65 $W\,m^{-1}\,K^{-1}$), which also suppresses lateral heat dissipation, so hot electrons (~2,800 K) become spatially localized at the centre of the suspended graphene under modest electric fields (~0.4 $V\,\mu m^{-1}$), greatly increasing the efficiency and brightness of the light emission. The bright visible thermally emitted light interacts with the reflected light from the separate substrate surface, giving interference effects that can be used to tune the wavelength of the emitted light.

We fabricated freely suspended graphene devices with mechanically exfoliated graphene flakes and, for the demonstration of scalability, we also used large-scale monolayer graphene grown on Cu foil using a low-pressure chemical-vapour-deposited (CVD) method and graphene directly grown on a SiO_2/Si substrate using a plasma-assisted CVD method[24]. Details of the sample fabrication process and characterizations of the mechanically exfoliated and CVD-grown graphene are provided in Supplementary Section 1. Representative suspended graphene devices are presented in Fig. 1a (Supplementary Fig. 2).

Figure 1b shows the experimental set-up used to investigate light emission from electrically biased suspended graphene under vacuum (<10^{-4} torr) at room temperature. A clean graphene channel and reliable contacts were achieved using a current-induced annealing method[25] (Supplementary Section 2). The suspended graphene channel begins to emit visible light at its centre once the source–drain bias voltage (V_{SD}) exceeds a threshold value, and its brightness and area of emission increase with V_{SD}. The brightest spot of the emission is always located at the centre of the suspended graphene, which coincides with the location of maximum temperature[10] (Supplementary Section 3). We observed bright and stable visible light emission from hundreds of electrically biased suspended graphene devices. Figure 1c–f presents optical microscope images of visible light emission from mechanically

[1]Department of Physics and Astronomy, Seoul National University, Seoul 151-747, Republic of Korea. [2]Department of Mechanical Engineering, Columbia University, New York, New York 10027, USA. [3]School of Physics, Konkuk University, Seoul 143-701, Republic of Korea. [4]Department of Physics, Sogang University, Seoul 121-742, Republic of Korea. [5]Department of Physics and Graphene Research Institute, Sejong University, Seoul 143-747, Republic of Korea. [6]Department of Electrical Engineering, Columbia University, New York, New York 10027, USA. [7]Department of Physics, Columbia University, New York, New York 10027, USA. [8]Korea Research Institute of Standards and Science, Daejeon 305-340, Republic of Korea. [9]Micro and Nanotechnology Lab and Department of Electrical and Computer Engineering, University of Illinois at Urbana-Champaign, Urbana, Illinois 61801, USA. [10]Department of Electrical Engineering, Stanford University, Stanford, California 94305, USA. [11]Department of Nano Science, University of Science and Technology, Daejeon 305-350, Republic of Korea. [12]Center for Subwavelength Optics, Seoul National University, Seoul 151-747, Republic of Korea; [†]Present addresses: Department of Physics, The University of Texas at Austin, Austin, Texas 78712, USA (Y.C.); Department of Engineering, University of Cambridge, Cambridge CB3 0FA, UK (D.Y.); Intel Corporation, Hillsboro, Oregon 97124, USA (V.E.D.); Department of Applied Physics, Stanford University, Stanford, California 94305, USA and SLAC National Accelerator Laboratory, 2575 Sand Hill Road, Menlo Park, California 94025, USA (T.F.H.). [‡]These authors contributed equally to this work. *e-mail: mhbae@kriss.re.kr; yk2629@columbia.edu; parkyd@phya.snu.ac.kr

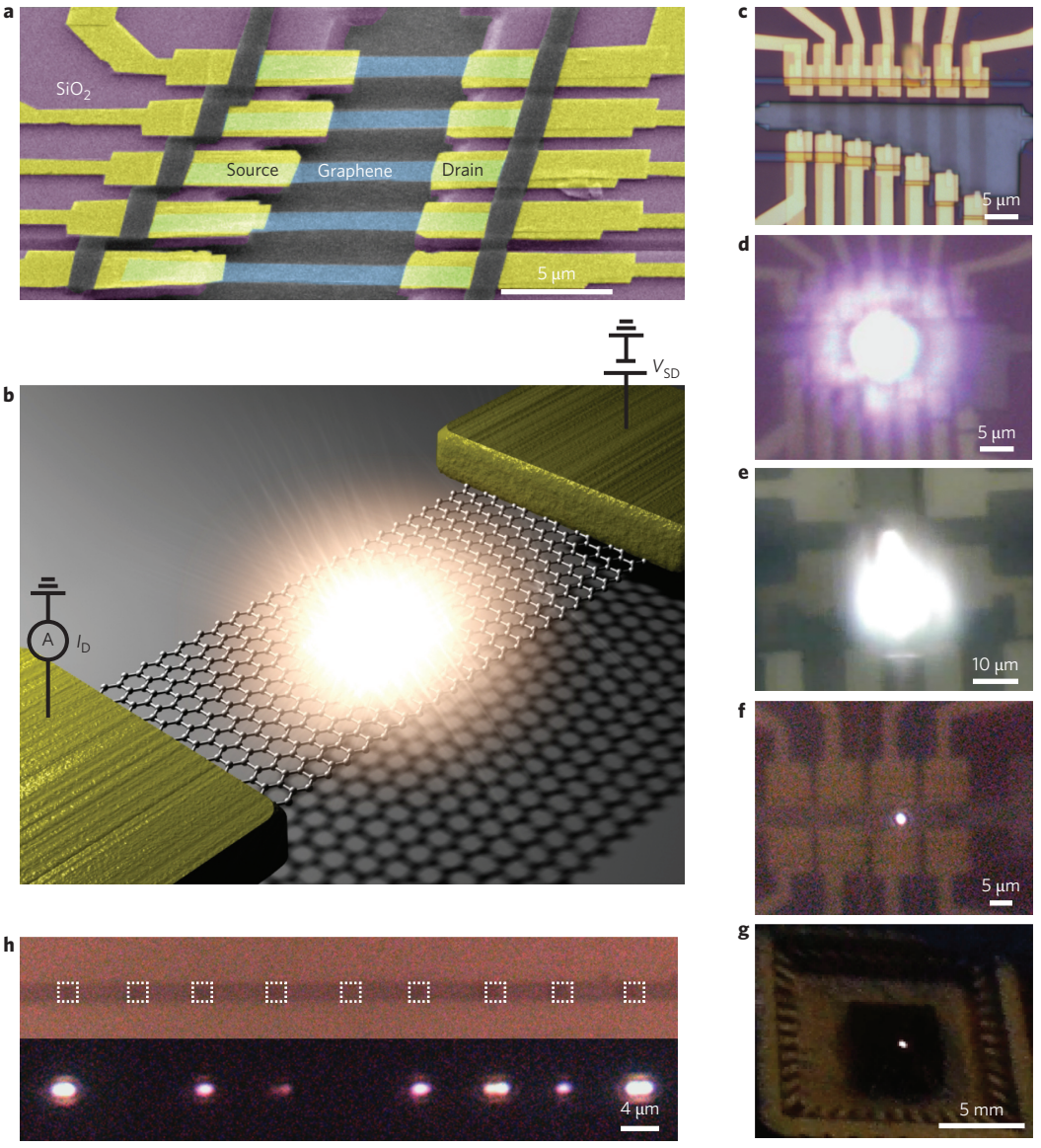

Figure 1 | Bright visible light emission from electrically biased suspended graphene. a, False-colour scanning electron microscopy image of suspended monolayer graphene devices. **b**, Schematic illustration of electrically biased suspended graphene and light emission from the centre of the graphene. **c**–**f**, Micrographs of bright visible light emission from suspended mechanically exfoliated graphene: few-layer graphene (L = 6.5 μm, W = 3 μm) at zero bias (**c**) and V_{SD} = 2.90 V (**d**); multilayer graphene (L = 14 μm, W = 40 μm) at V_{SD} = 7.90 V (**e**); monolayer graphene (L = 5 μm, W = 2 μm) at V_{SD} = 2.58 V (**f**). **g**, Optical image of remarkably bright visible light emission from suspended mechanically exfoliated few-layer graphene, which is visible even to the naked eye, without additional magnification. **h**, Micrograph of multiple parallel suspended CVD few-layer graphene devices (the dashed-line boxes highlight each graphene device with L = 2 μm and W = 2 μm) under zero bias (upper image) and seven spots of bright visible light emission from parallel suspended CVD graphene devices at V_{SD} = 6.42 V (lower image) under ambient conditions.

exfoliated few-layer (Fig. 1c,d), multilayer (Fig. 1e) and monolayer (Fig. 1f) graphene devices (Supplementary Movies 1–3). The emitted visible light is so intense that it is visible even to the naked eye, without additional magnification (Fig. 1g and Supplementary Movie 4). An array of electrically biased multiple parallel-suspended CVD few-layer graphene devices exhibit multiple bright visible light emission under ambient conditions, as shown in Fig. 1h (see Supplementary Movie 5 for light emission under vacuum for more stable and reproducible bright visible light emission). The observation of stable, bright visible light emission from large-scale suspended CVD graphene arrays demonstrates the great potential for the realization of complementary metal-oxide-semiconductor (CMOS)-compatible, large-scale graphene light emitters in display modules and hybrid silicon photonic platforms with industry vacuum encapsulation technology[26].

For the optical characterization of visible light emission from suspended graphene, we simultaneously collected emission spectra and performed Raman spectroscopy at various values of V_{SD} with zero gate bias, using the set-up presented in Supplementary Section 4. The emission spectra of devices suspended over trenches with depths D ranging from 900 to 1,100 nm exhibit multiple peaks in the range ~1.2–3 eV, as shown by the symbols in Fig. 2a (monolayer) and 2b (trilayer graphene). These strong multiple light-emission peaks are interesting, especially for the monolayer graphene (length L = 6 μm, width W = 3 μm) shown in Fig. 2a, because graphene does not have an intrinsic bandgap and its light spectrum is expected to be that of a featureless grey body radiation[8,9]. Similarly, multiple strong light-emission peaks were observed from tens of different suspended graphene devices with different numbers of layers and $D \approx$ 800–1,000 nm (Supplementary

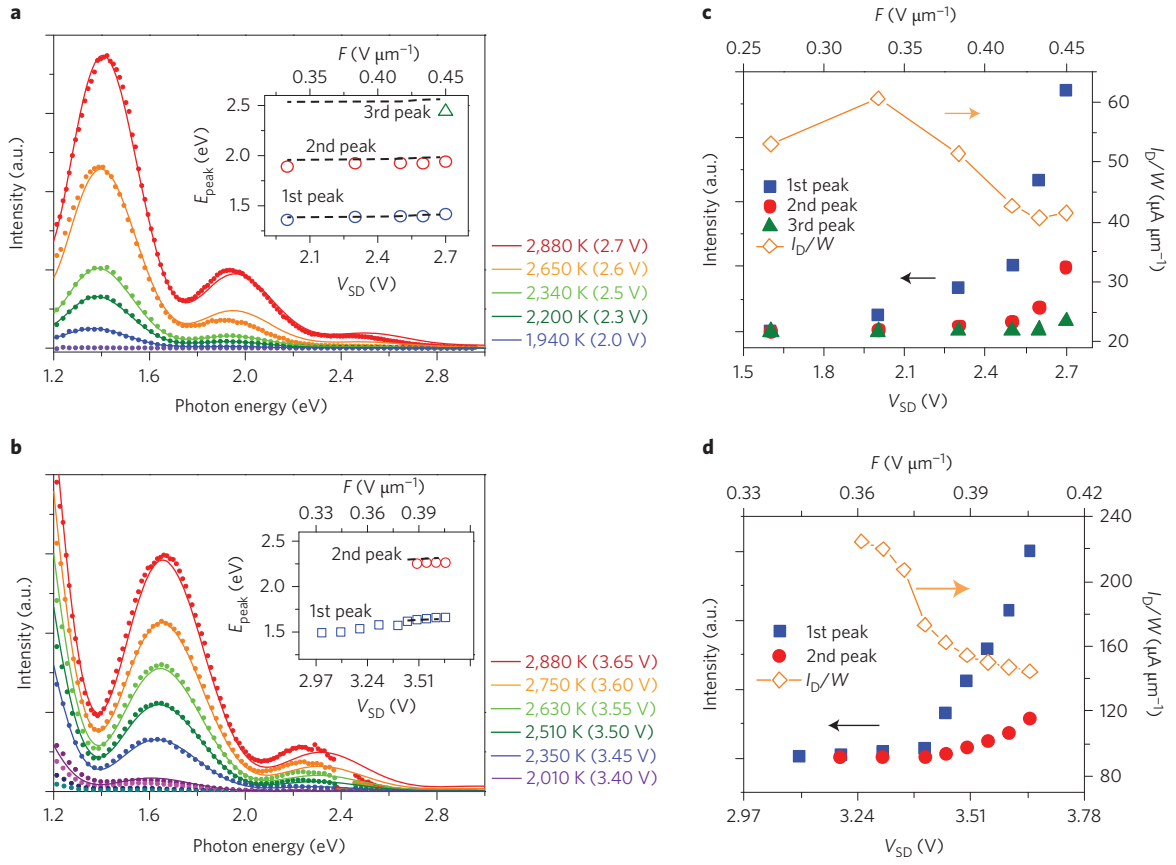

Figure 2 | Spectra of visible light emitted from electrically biased suspended graphene. a,**b**, Visible light emission spectra (symbols) of suspended mechanically exfoliated monolayer (L = 6 μm, W = 3 μm, **a**) and trilayer (L = 9 μm, W = 3 μm, **b**) graphene at various source–drain bias voltages (V_{SD}), exhibiting multiple strong emission peaks. In **a**, from top to bottom, V_{SD} = 2.7, 2.6, 2.5, 2.3, 2 and 1.6 V. In **b**, from top to bottom, V_{SD} = 3.65, 3.6, 3.55, 3.5, 3.45, 3.4, 3.3, 3.2 and 3.1 V. The visible light emission spectra can be well fitted by simulating the interference effect on the thermal radiation spectrum from the suspended graphene (solid curves), which allows for the estimation of the approximate electron temperature T_e of the suspended graphene (legend key). Insets (**a**,**b**): emission-peak energies as a function of V_{SD} and applied electric field ($F = V_{SD}/L$). Dashed lines: calculated peak energies based on the interference effect of thermal radiation. **c**,**d**, Integrated intensity of each emission peak and the electrical current I_D for suspended mechanically exfoliated monolayer (**c**) and trilayer (**d**) graphene versus V_{SD} (equivalently, the applied electric field). The current I_D and corresponding applied electrical power decrease with increasing V_{SD}, whereas the intensities of the emission peaks increase rapidly.

Fig. 10a,b). The multiple light-emission peaks in the visible regime are rather insensitive to the number of layers (Supplementary Section 5). On the other hand, the visible light emission spectra observed from suspended graphene devices with relatively shallow trenches ($D \approx 80$–300 nm)[8,9] are featureless and grey body radiation-like in the visible range of the spectrum (~1.2–3 eV) (Supplementary Fig. 10c,d). These results indicate that the existence of peaks at certain light-emission energies strongly depends on D rather than the number of graphene layers or the electronic band structure (Supplementary Sections 5 and 6).

To understand the multiple light emission peaks and significant spectral modulation caused by changes in D, we consider the interference effects between the light emitted directly from the graphene and the light reflected from the substrate (air/Si interface), as illustrated schematically in Fig. 3a. We find the relation between D and the energy separation between two consecutive destructive interferences to be

$$\Delta(D) = \frac{1{,}239.8\ \text{nm}}{2D}\text{eV} \qquad (1)$$

According to equation (1), $\Delta \approx 0.6$ eV for $D \approx 1{,}000$ nm, which is in agreement with our measurements (Fig. 2a,b). To confirm this correlation we simulated the spectral modulation based on the interference[27] of the thermal radiation from the suspended graphene (see Methods and Supplementary Section 5). Figure 3b presents simulated spectra in the visible range for various trench depths at an electron temperature T_e of 2,850 K, where the solid and dashed curves indicate constructive and destructive interferences, respectively (Supplementary Fig. 12). Strong interference effects enable us to selectively enhance the thermal radiation for a particular wavelength from electrically biased suspended graphene devices by appropriately engineering their trench depth (Fig. 3c). In addition, we find that the emission spectra in the visible range are (1) rather insensitive to the number of graphene layers n for $n \approx 1$–3 and (2) not affected appreciably by the absorption and reflection due to the graphene layers (Supplementary Sections 5 and 6).

The simulated interference effects on the thermal radiation from suspended graphene (solid curves in Fig. 2a,b) are in good agreement with the experimental observations for both monolayer (Fig. 2a) and trilayer (Fig. 2b) devices, corresponding to mean trench depths of 1,070 nm and 900 nm, respectively. By comparing the light-emission spectra obtained from the experiments and those from the theoretical models, we estimate the maximum T_e of electrically biased suspended graphene at each V_{SD}, and find that T_e can approach ~2,800 K. The calculated peak positions (insets of Fig. 2a,b, dashed curves) and peak intensities as a function of V_{SD} are also in agreement with the experimental data

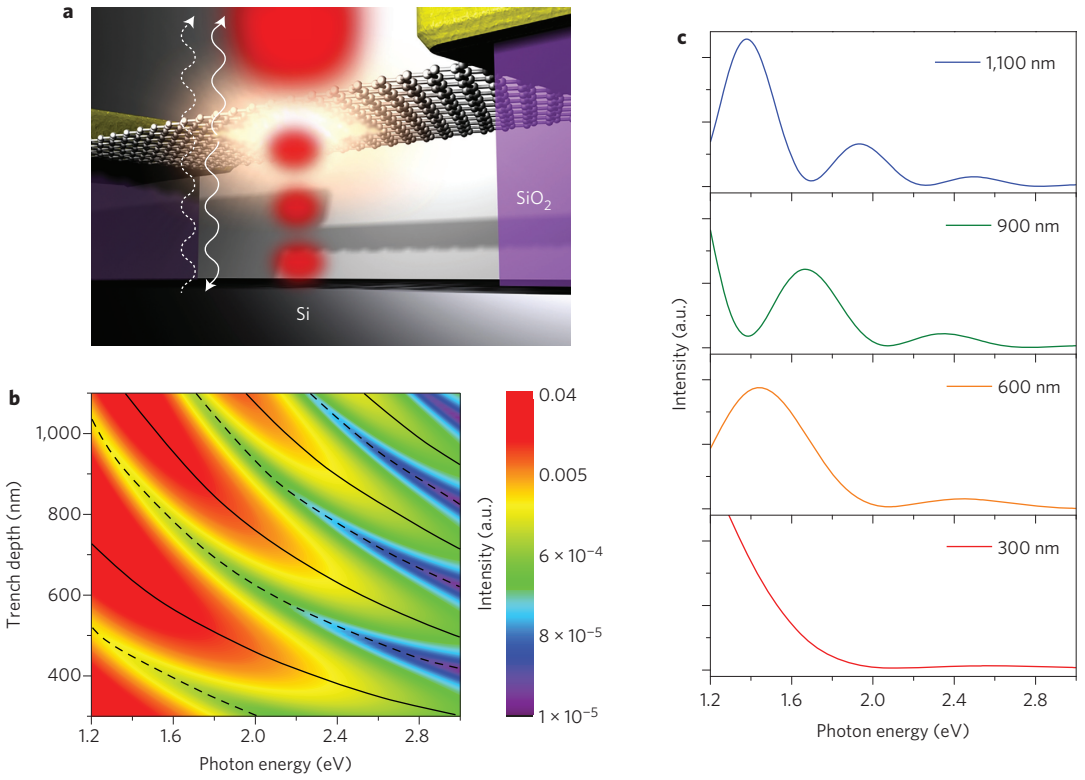

Figure 3 | Simulated spectra of radiation from electrically biased suspended graphene. a, Schematic illustration of interference between reflected (dashed arrow) and thermal radiation originating directly from graphene suspended over a trench (solid arrow). Red shading represents light intensity enhancement from a constructive interference effect. **b**, Simulated intensity of thermal radiation from suspended graphene as a function of trench depth D and photon energy at a constant electron temperature (2,850 K). Solid curves (dashed curves) represent the conditions for constructive (destructive) interference depending on the trench depth and photon energy. **c**, Simulated emission spectra of electrically biased suspended graphene with various trench depths. The strong interference effect allows for engineering the thermal radiation spectra in the visible range.

(Fig. 2c,d, symbols). The light-emission intensity increases rapidly with increasing V_{SD} when V_{SD} is beyond a certain threshold, as shown in Fig. 2c,d. Interestingly, the emission intensity exhibits a strong correlation with the applied electric field ($F = V_{SD}/L$) rather than with the applied electrical power ($P = V_{SD} \times I_D$, where I_D is the drain current) (Supplementary Fig. 13). In fact, we observe a rapid increase in light-emission intensity for an electric field strength above a certain critical point (~0.4 V μm^{-1}) in the suspended mechanically exfoliated mono/trilayer graphene devices, even when the current and applied electrical power are decreased at constant V_{SD}, because of the thermal annealing effect[28] or burning of the edge of the graphene at high temperatures[29]. This unconventional behaviour is attributed to the accumulation of hot electrons and hot graphene optical phonons (OPs) above the critical electric field (~0.4 V μm^{-1}) in the suspended graphene. It is likely that the suspension of the graphene (1) reduces the energy loss suffered by electric-field-induced hot electrons upon scattering from extrinsic sources such as charged impurities and remote polar phonons in the substrate and (2) prevents the cooling of the hot electrons and phonons via heat loss through the substrate. We note that suspended few- and multilayer graphene devices at modest electric fields ($F > 0.4$~0.5 V μm^{-1}) exhibit a current saturation behaviour followed by negative differential conductance (Supplementary Section 7), which has been known to be a signature of strong electron scattering by intrinsic OPs and non-equilibrium between OPs and acoustic phonons (APs) in carbon nanotubes[30].

To estimate the temperature of the suspended graphene and understand the observed correlation between thermal visible-light emission and applied field strength, we performed numerical simulations of electrical and thermal transport in suspended graphene devices under bias voltages (Supplementary Section 8). It is known that in substrate-supported graphene at high electrical fields, the OPs are in equilibrium with electrons at temperatures of up to ~2,000 K, but the OPs and APs are not in equilibrium with each other because the decay rate of OPs to APs is much slower than that of an OP to an electron–hole pair[8,9,15]. In a suspended graphene structure, the lattice temperature of the APs (T_{ap}) is much higher than that in graphene supported on a substrate, because heat cannot dissipate into the substrate[8]. This, in turn, results in higher temperatures of the OPs (T_{op}) and electrons (T_e). We express the increase in OP temperature as[30,31]

$$T_{op}(\alpha) = T_{ap} + \alpha(T_{ap} - T_0) \quad (2)$$

where T_0(=300 K) is the environmental temperature and $T_{op} = T_e$. Here, α is a constant determined from I_D–V_{SD} curves measured at various temperatures[32].

From numerical simulations based on our transport model[10,16], we determined the thermal conductivity (Fig. 4b), local T_{op} (T_e) (Fig. 4c) along the transport direction, and theoretical I_D–V_{SD} curves of the suspended monolayer graphene (Fig. 4a). In this model, the carrier mobility and thermal conductivity are expressed as $\mu(T_e) = \mu_0(T_0/T_e)^\beta$ and $\kappa(T_{ap}) = \kappa_0(T_0/T_{ap})^\gamma$, respectively, where $\mu_0 \approx 11{,}000$ cm^2 V^{-1} s^{-1} (~2,200 cm^2 V^{-1} s^{-1}), $\kappa_0 \approx 2{,}700$ W m^{-1} K^{-1} (~1,900 W m^{-1} K^{-1}), $\beta \approx 1.70$ (1.16) and $\gamma \approx 1.92$ (1.00) for the monolayer (trilayer) graphene (see Supplementary Section 8 for details of the trilayer graphene case). For both monolayer and trilayer graphenes, the estimated thermal conductivity is lowest at the centre, with $\kappa \approx 65$ W m^{-1} K^{-1} (~250 W m^{-1} K^{-1}) for

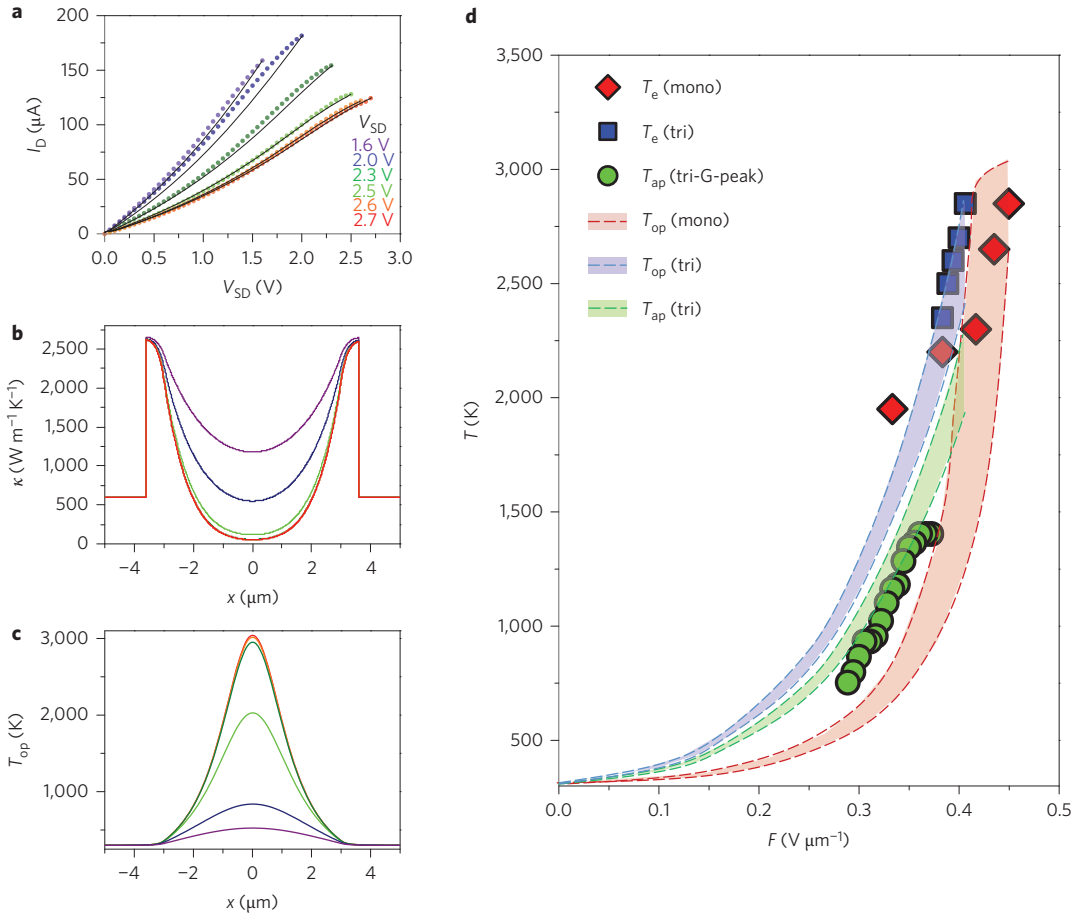

Figure 4 | Electrical and thermal transport in electrically biased suspended graphene. a, I_D–V_{SD} relation (symbols) for suspended mechanically exfoliated monolayer graphene obtained during the measurement of visible light emission spectra (presented in Fig. 2a). Solid curves: calculated results based on the transport model. **b**,**c**, Estimated thermal conductivities (**b**) and electron and optical phonon temperature ($T_{op} = T_e$) profiles (**c**) as functions of position along the transport direction for the upper bounds depicted in **d**. Here, $x = \pm 3$ μm are the boundaries between the graphene and the metal electrodes. **d**, Various peak temperatures at the centre of the graphene as functions of the electric field F in suspended mechanically exfoliated monolayer and trilayer graphene devices. The symbols represent the electron temperatures T_e determined from the thermal light-emission spectra and the acoustic phonon temperatures T_{ap} determined from the G-peak shifts in the Raman signals. Shaded regions bounded by two dashed curves were obtained based on the transport model. Upper and lower bounds account for the uncertainty in the width of the suspended graphene under high bias (Supplementary Section 8).

$T_{ap} \approx 1{,}800 \pm 300$ K ($\sim$1,700 $\pm$ 200 K) in the monolayer (trilayer) case, as shown in Fig. 4b. Furthermore, the highest T_e and T_{op} (the values at the centre of the suspended monolayer graphene channel) can be estimated to be $\sim$3,000 K, whereas T_{ap} is $\sim$2,200 K, as shown in Fig. 4c,d and Supplementary Table 2. T_e and T_{op}, estimated by our transport model when parameter α in equation (2) is set to 0.39 and 0.30 for monolayer and trilayer graphene devices, respectively, are in good agreement with the value of T_e extracted from the light-emission spectra (Fig. 2a,b). We could also obtain T_{ap} from the G-peak shift[33] in the Raman spectra, as shown in Fig. 4d (Supplementary Section 8A). However, the thermal radiation from electrically biased suspended graphene becomes significantly stronger than the Raman signal with increasing V_{SD}, which places an upper bound on the temperature ($\sim$1,500 K) that can be extracted via Raman spectroscopy (see Supplementary Section 8C for analysis of CVD graphene cases).

Finally, we considered the thermal radiation efficiency of the electrically biased suspended graphene based on a carefully calibrated spectrometer (see Methods). To estimate the energy dissipation via thermal radiation across all wavelengths from electrically biased suspended graphene, we calculated the ratio of the radiated power P_r, obtained using the Stefan–Boltzmann law from the measured electron temperature, to the applied electrical power P_e (Supplementary Section 9). In the considered case of maximum thermal radiation power (corresponding to $T_e \approx 2{,}800$ K) for monolayer and trilayer graphenes, we obtained thermal radiation efficiencies (P_r/P_e) of $\sim 4.45 \times 10^{-3}$ and $\sim 3.00 \times 10^{-3}$, respectively. These efficiencies are three orders of magnitude higher than those of graphene devices supported on SiO_2[8,9]. We expect a wavelength-dependent further enhancement of radiation efficiency in atomically thin graphene from applying radiation spectrum engineering approaches such as optical cavities, photonic crystals and hybrids with optical gain mediums.

Graphene is mechanically robust under high current densities and at high temperatures, with an abrupt decrease in thermal conductivity. These properties facilitate the spatially localized accumulation of hot electrons ($\sim$2,800 K) in an electrically biased suspended graphene layer, making graphene an ideal material to serve as a nanoscale light emitter. Furthermore, the broadband emission spectrum tunability that can be achieved by exploiting the strong interference effect in atomically flat suspended graphene allows for the realization of novel large-scale, atomically thin, transparent and flexible light sources and display modules. The graphene visible light emitter may open the door to the development of fully integrated graphene-based optical interconnects.

Methods

Methods and any associated references are available in the online version of the paper.

Received 17 November 2014; accepted 6 May 2015; published online 15 June 2015

References

1. Bonaccorso, F., Sun, Z., Hasan, T. & Ferrari, A. C. Graphene photonics and optoelectronics. *Nature Photon.* **4,** 611–622 (2010).
2. Bao, Q. & Loh, K. P. Graphene photonics, plasmonics, and broadband optoelectronic devices. *ACS Nano* **6,** 3677–3694 (2012).
3. Gan, X. *et al.* Strong enhancement of light–matter interaction in graphene coupled to a photonic crystal nanocavity. *Nano Lett.* **12,** 5626–5631 (2012).
4. Gan, X. *et al.* Chip-integrated ultrafast graphene photodetector with high responsivity. *Nature Photon.* **7,** 883–887 (2013).
5. Koppens, F. H. L. *et al.* Photodetectors based on graphene, other two-dimensional materials and hybrid systems. *Nature Nanotech.* **9,** 780–793 (2014).
6. Liu, M. *et al.* A graphene-based broadband optical modulator. *Nature* **474,** 64–67 (2011).
7. Grigorenko, A. N., Polini, M. & Novoselov, K. S. Graphene plasmonics. *Nature Photon.* **6,** 749–758 (2012).
8. Berciaud, S. *et al.* Electron and optical phonon temperatures in electrically biased graphene. *Phys. Rev. Lett.* **104,** 227401 (2010).
9. Freitag, M., Chiu, H-Y., Steiner, M., Perebeinos, V. & Avouris, P. Thermal infrared emission from biased graphene. *Nature Nanotech.* **5,** 497–501 (2010).
10. Dorgan, V. E., Behnam, A., Conley, H. J., Bolotin, K. I. & Pop, E. High-field electrical and thermal transport in suspended graphene. *Nano Lett.* **13,** 4581–4586 (2013).
11. Lui, C. H., Mak, K. F., Shan, J. & Heinz, T. F. Ultrafast photoluminescence from graphene. *Phys. Rev. Lett.* **105,** 127404 (2010).
12. Brida, D. *et al.* Ultrafast collinear scattering and carrier multiplication in graphene. *Nature Commun.* **4,** 1987 (2012).
13. Tomadin, A., Brida, D., Cerullo, G., Ferrari, A. C. & Polini, M. Nonequilibrium dynamics of photoexcited electrons in graphene: collinear scattering, Auger processes, and the impact of screening. *Phys. Rev. B* **88,** 035430 (2013).
14. Lee, C., Wei, X., Kysar, J. W. & Hone, J. Measurement of the elastic properties and intrinsic strength of monolayer graphene. *Science* **321,** 385–388 (2008).
15. Chae, D-H., Krauss, B., von Klitzing, K. & Smet, J. H. Hot phonons in an electrically biased graphene constriction. *Nano Lett.* **10,** 466–471 (2010).
16. Bae, M-H., Ong, Z-Y., Estrada, D. & Pop, E. Imaging, simulation, and electrostatic control of power dissipation in graphene devices. *Nano Lett.* **10,** 4787–4793 (2010).
17. Engel, M. *et al.* Light–matter interaction in a microcavity-controlled graphene transistor. *Nature Commun.* **3,** 906 (2012).
18. Pop, E. Energy dissipation and transport in nanoscale devices. *Nano Res.* **3,** 147–169 (2010).
19. Chen, J. H. *et al.* Charged-impurity scattering in graphene. *Nature Phys.* **4,** 377–381 (2008).
20. Chen, J-H., Jang, C., Xiao, S., Ishigami, M. & Fuhrer, M. S. Intrinsic and extrinsic performance limits of graphene devices on SiO_2. *Nature Nanotech.* **3,** 206–209 (2008).
21. Bolotin, K. I. *et al.* Ultrahigh electron mobility in suspended graphene. *Solid State Commun.* **146,** 351–355 (2008).
22. Kim, Y. D. *et al.* Focused-laser-enabled p–n junctions in graphene field-effect transistors. *ACS Nano* **7,** 5850–5857 (2013).
23. Pop, E., Varshney, V. & Roy, A. K. Thermal properties of graphene: fundamentals and applications. *MRS Bull.* **37,** 1273–1281 (2012).
24. Kim, Y. S. *et al.* Direct integration of polycrystalline graphene into light emitting diodes by plasma-assisted metal-catalyst-free synthesis. *ACS Nano* **8,** 2230–2236 (2014).
25. Qi, Z. J. *et al.* Electronic transport in heterostructures of chemical vapor deposited graphene and hexagonal boron nitride. *Small* **11,** 1402–1408 (2014).
26. Park, J-S., Chae, H., Chung, H. K. & Lee, S. I. Thin film encapsulation for flexible AM-OLED: a review. *Semicond. Sci. Technol.* **26,** 034001 (2011).
27. Yoon, D. *et al.* Interference effect on Raman spectrum of graphene on SiO_2/Si. *Phys. Rev. B* **80,** 125422 (2009).
28. Moser, J., Barreiro, A. & Bachtold, A. Current-induced cleaning of graphene. *Appl. Phys. Lett.* **91,** 163513 (2007).
29. Barreiro, A., Börrnert, F., Rümmeli, M. H., Büchner, B. & Vandersypen, L. M. K. Graphene at high bias: cracking, layer by layer sublimation, and fusing. *Nano Lett.* **12,** 1873–1878 (2012).
30. Pop, E. *et al.* Negative differential conductance and hot phonons in suspended nanotube molecular wires. *Phys. Rev. Lett.* **95,** 155505 (2005).
31. Mann, D., Pop, E., Cao, J., Wang, Q. & Goodson, K. Thermally and molecularly stimulated relaxation of hot phonons in suspended carbon nanotubes. *J. Phys. Chem. B* **110,** 1502–1505 (2006).
32. Mann, D. *et al.* Electrically driven thermal light emission from individual single-walled carbon nanotubes. *Nature Nanotech.* **2,** 33–38 (2007).
33. Bonini, N., Lazzeri, M., Marzari, N. & Mauri, F. Phonon anharmonicities in graphite and graphene. *Phys. Rev. Lett.* **99,** 176802 (2007).

Acknowledgements

The authors thank P. Kim, D-H. Chae, J-M. Ryu and A.M. van der Zande for discussions. This work was supported by the Korea Research Institute of Standards and Science under the auspices of the project 'Convergent Science and Technology for Measurements at the Nanoscale' (15011053), grants from the National Research Foundation of Korea (2014-023563, NRF-2008-0061906, NRF-2013R1A1A1076141, NRF-2012M3C1A1048861, 2011-0017605, BSR-2012R1A2A2A01045496 and NMTD-2012M3A7B4049888) funded by the Korea government (MSIP), a grant (2011-0031630) from the Center for Advanced Soft Electronics through the Global Frontier Research Program of MSIP, the Priority Research Center Program (2012-0005859), a grant (2011-0030786) from the Center for Topological Matters at POSTECH, the NSF (DMR-1122594), AFOSR (FA95550-09-0705), ONR (N00014-13-1-0662 and N00014-13-1-0464), Army Research Office (ARO) grant W911NF-13-1-0471 and the Qualcomm Innovation Fellowship (QInF) 2013. Computational resources were provided by the Aspiring Researcher Program through Seoul National University.

Author contributions

Y.D.K., Y.C., H.K., Y.L., D.Y., T.F.H. and H.C. performed the measurements. H.K., Y.D.K., P.K., S.L., J.H. and S.W.L. fabricated the devices. Y.S.K., S.L., J.H. and S-H.C. grew the CVD graphene. S-N.P. and Y.S.Y. provided calibrated black-body sources. M-H.B., V.E.D. and E.P. performed the simulations using the electro-thermal model. J.H.R. and C-H.P. developed a theoretical model for thermal emission beyond the Planck radiation formula and J.H.R. performed simulations based on it. M-H.B., Y.D.K. and Y.D.P. conceived the experiments. All authors discussed the results.

Additional information

Supplementary information is available in the online version of the paper. Reprints and permissions information is available online at www.nature.com/reprints. Correspondence and requests for materials should be addressed to Y.D.K., M-H.B. and Y.D.P.

Competing financial interests

The authors declare no competing financial interests.

Methods

Sample preparation. Pristine mechanically exfoliated graphene flakes were taken from Kish graphite (NGS Naturgraphit GmbH) using the standard Scotch-tape method. The number of layers of mechanically exfoliated graphene was confirmed by Raman spectroscopy and atomic force microscopy (AFM). We also used two kinds of large-scale CVD graphene layers to demonstrate the scalability of the graphene light emitter: (1) large-scale CVD monolayer graphene grown on Cu foil and transferred onto the SiO_2/Si substrate by etching the Cu foil with polymethyl methacrylate (PMMA) film; (2) large-scale CVD few-layer graphene, directly grown on the SiO_2/Si substrate using a plasma-assisted CVD technique, as shown in ref. 24. The direct growth technique provides uniform and large-scale few-layer graphene, without transfer-process-induced fractures, defects, wrinkles or impurities. See Supplementary Section 1 for details of sample characterization and the fabrication process for the suspended graphene devices. The devices tested in this work have lengths of $L \approx 1$–15 μm, widths of $W \approx 1$–40 μm and trench depths of $D \approx 80$–1,200 nm.

Acquiring optical images of visible light emission from graphene. The micrographs of bright visible light emission from graphene shown in Fig. 1c–f,h and Supplementary Movies 1–3 and 5 and 6 were acquired using a charge-coupled device (CCD) digital camera (INFINITY 2, Lumenera Coporation, exposure time of 100 ms) with a ×50 objective lens (Mitutoyo Plan Apo SL). The optical images of bright visible light emission from graphene shown in Fig. 1g and Supplementary Movie 4 were acquired using a digital camera (5 megapixels, 3.85 mm *f*/2.8 lens, Apple iPhone 4, high dynamic range (HDR) mode) without magnification.

Optical measurements. The Raman spectra were measured using the 514.5 nm line of an Ar ion laser or the 441.6 nm line of a He–Cd laser with a power of 500 μW. We used a ×50 objective lens (Mitutoyo Plan Apo SL, NA 0.42 and WD 20.3 mm) to focus the laser beam onto the sample, which was housed in a vacuum of $<10^{-4}$ torr at room temperature. A Jobin-Yvon Triax 320 spectrometer (1,200 groove/mm) and a CCD array (Andor iDus DU420A BR-DD) were used to record the spectra. The bright visible light emission spectra were measured using the same system. At each bias voltage, the Raman and light-emission spectra were measured sequentially, using a motorized flipper mount for a dichroic filter and an optical beam shutter (Thorlabs SH05). The throughput of the optical system was carefully calibrated using a calibrated black-body source (1,255 K, OMEGA BB-4A) and a tungsten filament (3,000 K, calibrated against the International System of Units in the Korea Research Institute of Standards and Science).

Stability of visible light emission from suspended graphene. In general, the stability of visible light emission from suspended graphene under ambient conditions is limited by oxidation at high temperatures[10]. Under vacuum environments, however, we observed stable and reproducible bright visible light emission from suspended graphene devices. We performed electrical transport measurements at various times during the bright visible light emission, and Raman spectroscopy before and after emission (Supplementary Section 3). From such experiments we concluded that the suspended graphene light emitters were not damaged during the light-emission process with modest electric fields. Furthermore, the non-diminishing, stable light emissions arising from a series of electrical-bias pluses (shown in Supplementary Movie 6) demonstrate the durability of the atomically thin light emitter and the reproducibility of the bright visible light emission phenomenon.

Interference effect on thermal radiation from suspended graphene. The visible light radiating from the surface of the graphene interferes with the light reflected from the Si surface. If we neglect the tiny fraction of light being reflected or absorbed by the graphene, then the interference-modulated intensity $I(\omega;D)$ is given by

$$I(\omega;D) = I_0(\omega)\left(\frac{1+|r(\omega)|^2}{2} + \mathrm{Re}\left[r(\omega)\exp(i2\omega D/c)\right]\right) \quad (3)$$

where $I_0(\omega)$ ($\approx \varepsilon\omega^3/(\exp(\hbar\omega/k_BT) - 1)$) is the intensity of thermal radiation from the graphene, $r(\omega)$ is the reflection coefficient of Si (~0.5 for the visible region), ω is the photon frequency, ε is the emissivity of graphene, D is the trench depth, k_B is the Boltzmann constant, T is the electron temperature and c is the speed of light. The interference pattern is partially washed out by any non-uniformity in the trench depth originating from any roughness or tilt of the Si and graphene surfaces and thermal vibration of the graphene. Thus, the measured light intensity $\langle I(\omega)\rangle_{avg}$ can be determined as the average of $I(\omega;D)$ over D. Under the assumption that the probability distribution of D obeys $P(D) \propto \exp[-(D - D_0)^2/2(\Delta D)^2]$, $\langle I(\omega)\rangle_{avg}$ has a similar form to equation (3) with $D = D_0$:

$$\langle I(\omega)\rangle_{avg} = I_0(\omega)\left(\frac{1+|r(\omega)|^2}{2} + e^{-2(\omega\Delta D/c)^2}\mathrm{Re}\left[r(\omega)\exp\left(i2\omega D_0/c\right)\right]\right) \quad (4)$$

where the additional factor $e^{-2(\omega\Delta D/c)^2}$, which represents the wavelength-dependent interference efficiency, allows for a much better fit to the experimental data than can be achieved using equation (3). By comparing our model, represented by equation (4), with the experimental data, we can obtain mean trench depths of $D_0 = 1{,}070$ nm and 900 nm and standard deviations of $\Delta D = 58$ nm and 45 nm for suspended mono- and trilayer graphene, respectively.